minerals

MDPI

Article

Dissolution Characteristics and Microstructure of Waste Pisha Sandstone Minerals in Alkaline Solutions

Changming Li [1,2,*], Haifeng Cheng [1], Yali Cao [1,3], Cong Ding [1], Dongyang Jia [1], Shunbo Zhao [1,2,*] and Chen Yang [2]

[1] International Joint Research Lab for Eco-Building Materials and Engineering of Henan, North China University of Water Resources and Electric Power, Zhengzhou 450045, China
[2] Collaborative Innovation Center for Efficient Utilization of Water Resources, North China University of Water Resources and Electric Power, Zhengzhou 450046, China
[3] School of Transportation and Engineering, Huanghe Jiaotong University, Jiaozuo 454950, China
* Correspondence: lichangming@ncwu.edu.cn (C.L.); sbzhao@ncwu.edu.cn (S.Z.); Tel.: +86-371-6566-7990 (C.L.)

Abstract: Waste Pisha sandstone (WPS) is the main damming material for the check dam in the Loss Plateau of northwest China. The dissolution characteristics of WPS in alkaline solutions were investigated as a basis for studying WPS modification materials and revealing the modification mechanism to further study the pozzolanic activity of WPS and the development of cementitious materials for concrete utilizing WPS. In this paper, WPS was milled and calcined at 600 °C, 700 °C, and 800 °C, respectively. After that, the activated WPS was immersed in 0.05, 0.1, 0.5, 1.0, 2.0, and 5.0 M NaOH solutions for leaching tests. The two curing temperatures of 20 °C and 80 °C were set, respectively. The ion concentration of Si, Al, and Ca in the alkaline solutions was determined using chemical titration, silicon–molybdenum blue colorimetric method, and graphite furnace atomic absorption spectrometry, respectively. After the leaching tests, the residues of WPS were characterized using XRD and SEM-EDS. The results show that the concentration of each ion in the leachate did not increase with leaching time but showed fluctuating variations with leaching time. Mechanochemical activation and thermal activation will promote the dissolution of minerals in alkaline solutions and increase the leaching efficiency of Si. However, the soluble Si in the leachate is not able to generate further gelling-like substances, limited by the total amount of available Ca in the mineral. WPS can dissolve more ions in higher concentrations of a NaOH solution, but the mineral crystallinity of its residue will be reduced. Higher curing temperatures can greatly increase the leaching efficiency of Si in a short time, which is better than thermal activation, and it can also promote the generation of newborn minerals and increase the crystallinity of minerals in WPS after leaching.

Keywords: waste Pisha sandstone minerals; dissolution characteristics; leaching efficiency; thermal and mechanochemical activation; leaching residues

Citation: Li, C.; Cheng, H.; Cao, Y.; Ding, C.; Jia, D.; Zhao, S.; Yang, C. Dissolution Characteristics and Microstructure of Waste Pisha Sandstone Minerals in Alkaline Solutions. *Minerals* **2023**, *13*, 378. https://doi.org/10.3390/min13030378

Academic Editors: Giacomo Russo, Enza Vitale, Manuela Cecconi and Chiharu Tokoro

Received: 16 January 2023
Revised: 4 March 2023
Accepted: 6 March 2023
Published: 8 March 2023

1. Introduction

Waste Pisha sandstone (WPS) is a special kind of rock located in northwestern China with an area of more than 12,000 km^2. WPS forms by an alternating sedimentary process of marine and continental facies during the Tertiary period [1–3]. WPS is mainly composed of feldspar, quartz, montmorillonite, illite, and mica [4–7]. The petrographic structure of WPS is porous cementation, with sandstone and siltstone in the clastic structure as the framework, and clay minerals, such as montmorillonite, illite, and mica, as fillers in the pores. The bond strength of WPS is very high when it is dry, but it would collapse into sand soon when immersed in water [8].

The soil erosion in the WPS area is very severest, and the soil erosion modulus reaches 30,000 to 40,000 t/(km^2·a) [9,10]. Many measures, such as sea-buckthorn flexible dams, biological engineering measures, check dams, and so on, have been taken to prevent soil erosion and repair the eco-environment. The conclusions of the published papers show

that the check dam achieved the highest work efficiency in the prevention and control of soil erosion among all measures [11,12]. A large number of check dams need to be built to prevent soil erosion, and the demand for damming materials for check dams is enormous. Compared with traditional materials used for the location check dams, WPS has a substantial economic advantage, is more available, and is environmentally friendly [2,13].

In order to modify the characteristics of WPS to collapse in water, and to supply the demand for construction materials for the construction of check dams in the WPS area, Li et al. investigated the possibility of developing low-cost supplementary cementitious materials using WPS. The compressive strength, pore structure, water resistance, and hydration products of alkali-activated WPS geopolymer were also studied in the paper [14–17]. On this basis, Yang et al. combined the gelling inhibitors and conducted field and laboratory tests for the demonstration project of the WPS-modified material check dam. The results showed that swelling in the modified WPS was suppressed [18]. However, the current technology for dam construction with modified materials is not yet complete. Indeed, few researchers pay attention to studying the dissolution characteristics of WPS in alkaline solutions.

It is necessary to fully understand the mineral dissolution characteristics of WPS to further study the pozzolanic activity of WPS and develop concrete cementing materials using WPS. Therefore, it would be a beneficial exploration to identify the mineral dissolution characteristics of WPS and reveal the modification mechanism of WPS [19,20]. It is known that milling and calcination could reduce the crystallinity of minerals [21–24], and the crystalline-to-amorphous transformation allows silicate minerals to dissolve more Si and Al monomers when dissolved in acidic or alkaline solutions [25–30]. On the other hand, the dissolution of silicates in acid or alkaline solutions results in the partial breakdown of the structure, usually experienced as the dissolution of the cations leaves a siliceous residue behind [31–33]. The dissolution rates of the silicates are frequently determined by measuring the concentration of Si in solution, which implies the measurement of the complete breakdown of the silicate structure [33]. The ions dissolved from the minerals react with other substances to produce newborn minerals or amorphous products such as gels.

In this paper, WPS was treated with thermal and mechanochemical activation, and the activated WPS was leached in alkaline solutions. In order to elucidate the modification mechanism of the modification materials, the ion concentration of Si, Al, and Ca in leachate and the mineral composition of residues after leaching were analyzed. In addition, an improved understanding of the dissolution characteristics and microstructure of WPS could be achieved, and the results could provide technical guidance for the production of modified WPS engineering materials with better performance.

2. Materials and Method

2.1. Materials

In this study, the WPS was used as raw material, taken from the Erlaohu basin in Zhunger Banner, Inner Mongolia, at the geographic coordinates of 110°36′2.74″ E and 39°47′38.79″ N. Samples were taken at a depth of 0.5 m within the trench surface and the floating soil was removed. The WPS samples were oven-dried at 105 °C for 12 h to remove the adsorbed water. Deionized water and sodium hydroxide pellets with a purity of >99.9% (from Tianjin Comeo Reagent Co., Ltd., Tianjin, China) were used to prepare alkaline solutions as the leaching agent.

2.2. Experiment Method

The activation of the raw material was carried out using mechanochemical activation alone, thermal activation alone, and thermal activation combined with mechanochemical activation. The labels of the raw materials after activation are shown in Table 1.

Table 1. The labeling for various activated WPS samples.

Series	Activation of WPS	Density/(kg·m^{-3})	Series	Activation of WPS	Density/(kg·m^{-3})
WPS	–	2530	SG *	Grinding	2670
SC6 †	600 °C	2523	SC6G ‡	600 °C and Grinding	2720
SC7	700 °C	2536	SC7G	700 °C and Grinding	2710
SC8	800 °C	2525	SC8G	800 °C and Grinding	2725

*: SG, the WPS sample was treated with grinding, †: SC, the WPS sample was calcined at 600 °C, 700 °C, or 800 °C, respectively, ‡: SCG, the WPS sample was calcined (at 600 °C, 700 °C, or 800 °C) and ground.

For the thermal activation, the WPS samples were put in an alumina crucible and then calcined in an electric chamber furnace at 600 °C, 700 °C, and 800 °C for 2 h, respectively (heating rate was 300 °C/h). After the temperature rose to the set temperature, a constant temperature check was performed to ensure that the temperature remained constant. After thermal treatment, cooling was performed rapidly by removing the crucibles from the furnace and spreading the material on a steel plate at ambient conditions. For the mechanochemical activation, the WPS samples were ground using an XM planetary ball mill with a milling time of 45 min.

In the study of hydrometallurgy, the residual solid was separated from the liquid after the solid had been leached in the leaching agent for a predetermined amount of time. The liquid is referred to as leachate, and the residual solid is known as the residue.

For the leaching test, 4 g of the solid sample was put into 250 mL plastic measuring cylinders, which had 200 mL of alkaline solutions. The type of solid and concentration of alkaline solutions were used as parameters in the leaching test. Two curing temperatures were set at 20 °C and 80 °C. Leaching time was set to 28 days at 20 °C and 3 days at 80 °C. The ion concentrations of Si, Al, and Ca in the leachate were measured at a temperature of 20 °C for 1, 3, 7, 14, and 28 days, and at an 80 °C temperature for 0.5, 1, and 3 days. The parameter in the leaching test is detailed in Table 2. WPS was immersed in deionized water for 28 days to be compared with thermally and mechanochemically activated WPS. When the leaching time was reached, the residues were separated from the leachate using quantitative filter paper (medium speed: 15–20 μm, filter speed (s) 35–70, ash content (%) $\leq$ 0.15) and dried at 105 °C for 6 h.

Table 2. Parameter of the leaching test.

Solid Type	Concentration of Alkaline Solutions/(mol/L)							Curing Age/(days)	
	0	0.05	0.1	0.5	1.0	2.0	5.0	20 °C	80 °C
WPS	Si, Ca	Si, Ca	Si, Ca, Al	Si, Ca	Si, Ca, Al	Si, Ca	Si, Ca, Al	1, 3, 7, 14, 28	0.5, 1, 3
SG	/	Si, Ca	Si, Ca, Al	Si, Ca	Si, Ca, Al	Si, Ca	Si, Ca, Al	1, 3, 7, 14, 28	/
SC6	/	Si, Ca	Si, Ca, Al	Si, Ca	Si, Ca, Al	Si, Ca	Si, Ca, Al	1, 3, 7, 14, 28	/
SC6G	/	Si, Ca	Si, Ca, Al	Si, Ca	Si, Ca, Al	Si, Ca	Si, Ca, Al	1, 3, 7, 14, 28	0.5, 1, 3
SC7G	/	/	/	/	Si, Ca, Al	/	Si, Ca, Al	1, 3, 7, 14, 28	/
SC8G	/	/	/	/	Si, Ca, Al	/	Si, Ca, Al	1, 3, 7, 14, 28	/

'/' symbol means that the parameter corresponding to this column was not used to perform the leaching test.

The concentration of Si was determined using the silicon–molybdenum blue colorimetric method: (1) Take 2 mL of the diluted test solution (100-fold dilution factor) in a test tube and add 5 mol/L sulfuric acid solution until the pH of the solution is between 1.0 and 2.0. Add the detection reagents (ammonium molybdate, stannous chloride) to the test tube and let stand for 15 min. After the color development in the solution is stable, a colorimetric test is performed using a JN-SZY-type spectrophotometer. The detection reagents and testing instruments were purchased from Zhengzhou Jinong Technology Co., Henan, China. Three parallel tests were conducted for each sample. (2) The analytical pure reagent of Na_2SiO_3-$9H_2O$ (from Tianjin Comeo Reagent Co., Ltd., China) was mixed with deionized water to configure a concentration of 0.5, 1, 2, 3, 4, and 5 mg/L silicon dioxide solution. These silicon dioxide solutions were determined according to the colorimetric

test mentioned above, and three parallel tests were conducted for each concentration of silicon dioxide solution. (3) The elemental Si standard curve values are shown in Table 3.

Table 3. The elemental Si standard curve values.

Conc of Si (mg/L)	0	0.5	1	2	3	4	5
Absorbance (L/(g·cm))	0	0.2265	0.4581	0.9155	1.3715	1.8668	2.2869

(Y = 0.4583X − 0.0006, R2 = 0.998; horizontal coordinate: concentration of Si; vertical coordinate: absorbance).

The concentration of Al was determined using graphite furnace atomic absorption spectrometry. The aluminum ions in solution were formed in the graphite tube of the graphite furnace in three stages including drying, ashing, and atomization to form the ground state atoms. The ground state atoms will absorb the characteristic spectral line (309.3 nm) that occurs from the aluminum hollow cathode lamp. The amount of absorption characteristic spectral lines is proportional to the content of Al in the sample. By measuring the intensity of the absorbed spectral lines and comparing it with the element Al standard curve, the concentration of aluminum ions in leachate can be quantitatively analyzed. The values of the elemental Al standard curves obtained from the tests are shown in Table 4. The testing instrument is a novAA 800D-type atomic absorption spectrometer, Analytik jena, Germany. Three parallel tests were conducted for each sample.

Table 4. The elemental Al standard curve values.

Conc of Al (μg/L)	0	25	50	75	100
Absorbance (L/(g·cm))	0	0.09196	0.15598	0.20917	0.27388

(Y = 0.0034130X − 0.0036834, R2 = 0.998; horizontal coordinate: concentration of Al; vertical coordinate: absorbance).

The concentration of Ca was determined using the Chinese standard GB/T 7476-1987, "Determination of Calcium in Water Quality EDTA Titration Method".

$$Leaching\ efficiency = \frac{M_L}{M_R} \times 100\% \quad (1)$$

where M_L is the Si/Al/Ca content of the leachate, which is obtained by multiplying the measured ion concentration in the leachate with the volume of the leachate. M_R is the total amount of Si/Al/Ca in the solid raw material, which is calculated using XRF data [30].

2.3. Characterization

Particle size distributions (PSDs) were measured with a Zetasizer Nano ZS90 type S laser beam granulometry, Malvern, England. The WPS samples were determined with X-ray fluorescence (XRF) using an ARL PERFORM'X-type XRF spectrometer, Thermo Scientific, Switzerland. The morphological and compositional alternation of the activated WPS samples after leaching (residues) were studied using scanning electron microscopy (SEM), energy dispersive X-ray spectroscopy (EDS) point analyses, and X-ray diffractometry (XRD). XRD data were recorded using a Simens/Bruker D5000-type diffractometer (Texas, USA) with C_uK_α radiation in θ-θ reflection configuration (λ = 1.54 Å). The X-ray tube was operated at 40 kV and 30 mA. All scans were measured over an angular range of 5 to 60° 2θ at a rate of 2°/min and step size of 0.02°. The microstructure morphology and microzone composition analysis of the residues was analyzed using ZEISS Sigma 300-type scanning electron microscopy, Germany.

3. Results and Discussion

3.1. Material Properties

The detailed chemical compositions of the raw materials are shown in Table 5. Figure 1 shows the effect of mechanochemical and thermal treatment on the particle sizes of WPS. Compared to the particle size distribution (PSD) curves of the samples without

milling treatment WPS (d50 = 730 μm) and SC8 (d50 = 1200 μm), the entire PSD curves of mechanochemically activated SG (d50 = 600 μm) and SC8G (d50 = 860 μm) shifted to smaller particle sizes based on the grinding process. The PSD curves of the thermally activated SC8 were found to be coarser than WPS. The reason for this shift is likely that thermal activation tends to agglomerate clay minerals and that the occurrence of sintering and particle agglomeration increases particle size. Similar results could be obtained by comparing the PSD curves of SC6G (640 μm) and SC8G (d50 = 860 μm). The conclusions discussed above are consistent with earlier reports on the effect of grinding and heating on particle sizes of other clay minerals [34,35]. In addition, for SC6G and SC8G, the d50 was observed to be 640 μm and 860 μm, respectively; however, the d50 for SC7G was 550 μm, which did not increase linearly with calcination temperature.

Table 5. Chemical composition of original and thermally activated WPS (%).

Sample	SiO_2	Al_2O_3	CaO	Na_2O	K_2O	MgO	Fe_20_3	TiO_2	P_2O_5	Other
WPS	61.50	17.96	5.75	1.35	2.67	4.36	5.16	0.83	0.19	0.23
SC6	62.27	17.90	5.01	1.56	3.07	4.07	4.90	0.77	0.21	0.24
SC8	61.63	18.03	5.43	1.62	3.09	4.04	4.91	0.76	0.21	0.28

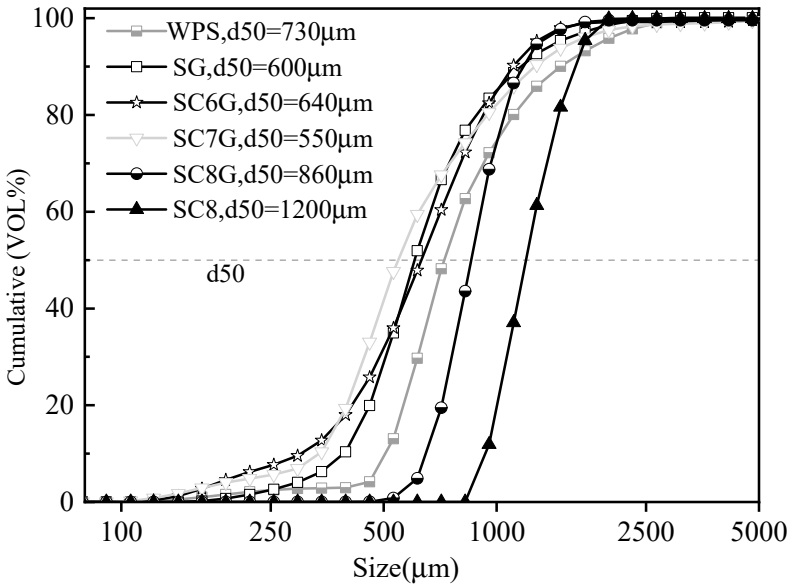

Figure 1. Cumulative particle size distribution curves of the untreated, mechanochemically, and thermally activated WPS.

Figure 2 shows that the montmorillonite diffraction peak (001) of activated WPS almost disappeared compared to its untreated state. This result is inconsistent with earlier reports on the thermal activation of montmorillonite [35]. Interlayer water of montmorillonite is removed after calcination at 800 °C, which leads to a reduction in the crystalline surface spacing but does not cause the disappearance of its diffraction peaks. This difference may be explained by the fact that the lattice of montmorillonite has disintegrated under the combined effect of calcination and intense grinding. A slight increase in the intensity of muscovite peaks was observed, which further confirmed the disintegration of the montmorillonite lattice [35]. Mechanochemical and thermal treatment with dry grinding and calcination resulted in a broadening and lowering of quartz and feldspar peak intensities, indicating a reduction in WPS crystallinity and a progressive amorphization of the minerals among WPS. In addition, for the thermally and mechanochemically activated WPS, a significant disappearance of the calcite peaks was observed.

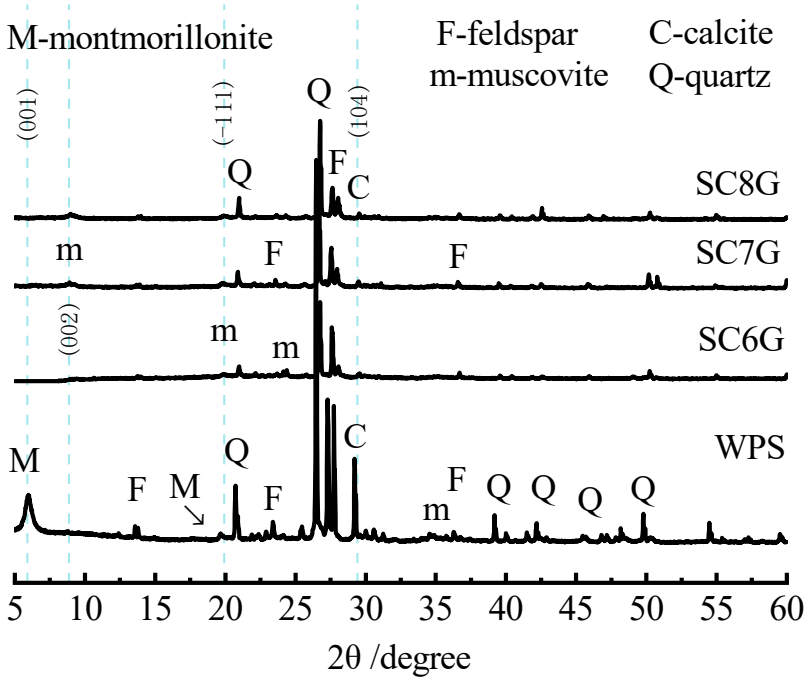

Figure 2. XRD of mechanochemically and thermally activated WPS.

3.2. Effect of Mechanochemical Activation on the Dissolution of Si, Al, and Ca

There are various interactions that occur in the WPS/leaching agent system, which include precipitation/dissolution, complex formation, adsorption/desorption, and redox reactions, which are bound to control the mobilization of Si, Al, and Ca in the leachate [30]. The dissolution process of WPS is very complicated. In order to simplify the process, the leaching efficiencies of Si, Al, and Ca were considered to be a relationship, which reflects the amounts of Si, Al, and Ca dissolved out from minerals and the amounts of free Si, Al, and Ca in leachates consumed by involving secondary mineral formation [36,37].

To highlight the effect of mechanochemical activation on the ion leaching efficiency, the grinding efficiency (the ratio of the leaching efficiency of each ion of the ground sample to the leaching efficiency of each the unground sample multiplied by 100%) was defined and presented in the figure as a scatter.

The variation in the leaching efficiencies of Si, Al, and Ca of WPS and SG in 1.0 M NaOH solution at 20 °C are shown in Figure 3. It can be seen that there is a fluctuated variation in the leaching efficiency of Si as a function of leaching time. The grinding efficiencies were 124%, 106%, and 149% for 1, 3, and 28 days, respectively. This may be due to destruction of the crystalline lattice of minerals caused by the grinding, which allows the release of more Si and Al ions [34]. Therefore, it seems to be possible to deduce that the leaching efficiency curve corresponding to SG should be higher than that corresponding to WPS. However, the result that the grinding efficiencies were 66% and 76% for 7 and 14 days, respectively, is inconsistent with the deduction. This result seems to be attributed to the fact that the mechanochemical activation not only makes the Si ions more soluble from the mineral surface but also promotes the chemical reactions that occur between the solid particle surface and Si, Al, and Ca in the leachate. In addition, the rates of the chemical reactions may be influenced by variations in the concentration of each ion in the leachate or by changes in the solid surface. There was a lack of correlation observed between WPS and SG in terms of the leaching efficiency of Al.

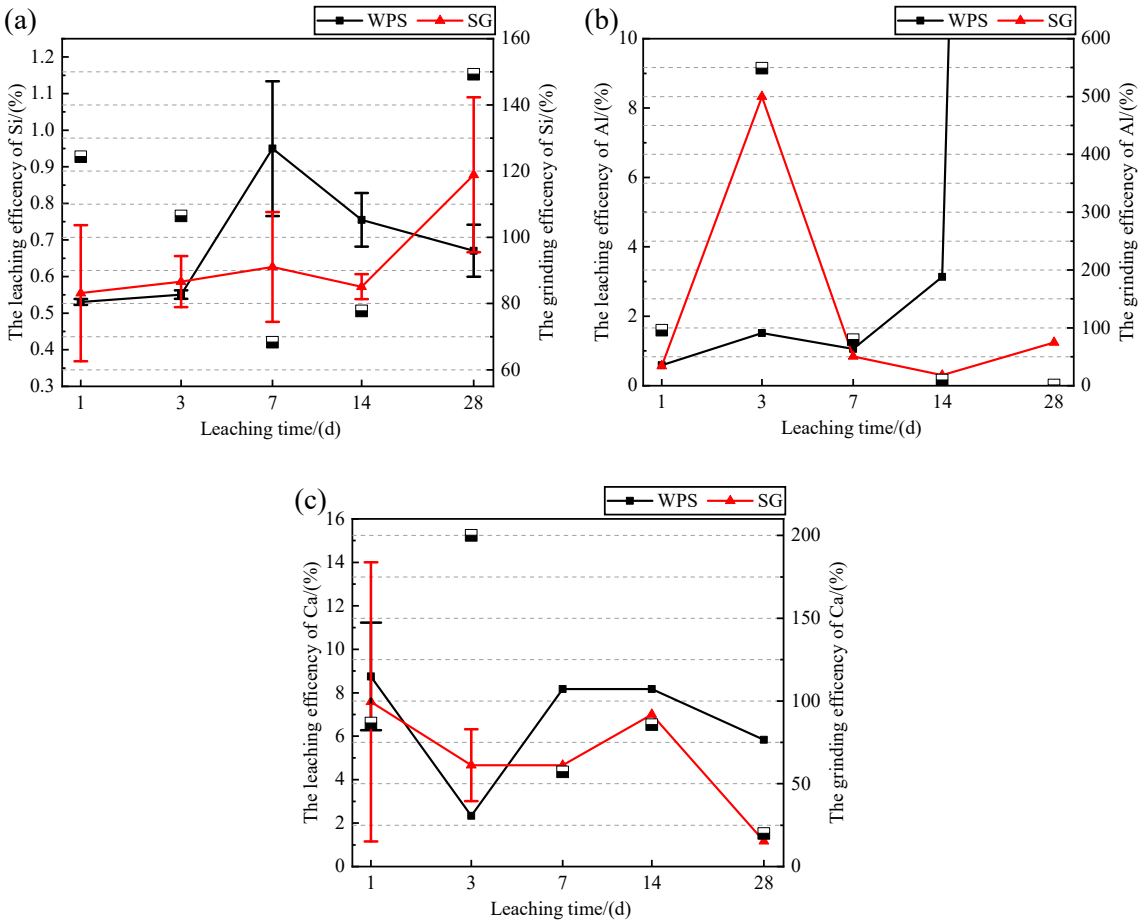

Figure 3. The grinding efficiency between WPS and SG. (**a**) The ion leaching efficiency of Si, (**b**) the ion leaching efficiency of Al, and (**c**) the ion leaching efficiency of Ca. (The plots in the figure correspond to the grinding efficiency on the right axis).

A significant decrease occurred in the leaching efficiency of Ca over the range of 1 to 3 days was observed (Figures 3c and 4c). This phenomenon could be attributed to the fact that the easily soluble oxide of calcium dissolved quickly in the leaching agent, which caused a higher value of the leaching efficiency of Ca [30], and subsequently, the free Ca ions in the leachate were consumed by reacting with other ions in leachates. In addition, Figure 3c also shows that with mechanochemical treatment, the leaching efficiency of Ca in the leachate of SG decreased compared to its untreated state WPS. This decrease is likely due to the loss of easily soluble oxide of calcium on the surface of WPS caused by the grinding process [34].

The variation in the leaching efficiencies of Si, Al, and Ca of SC6 and SC6G in 1.0 M NaOH solution at 20 °C are shown in Figure 4. It can be seen that the grinding efficiencies of Si are all less than 100%, indicating that SC6G leaches less Si in leachates than SC6. In terms of particle size, smaller particles, which have a larger area to interact with the liquid, have a thinner boundary layer and can leach faster [38]; however, this feature was not observed in the leaching efficiencies of Si and Al. This indicates that mechanochemical activation reduced the size of the particles, increased the rate of dissolution of ions dissolved from minerals, and also accelerated the rate of reactions between the species on the solid surface and the ions in the leachate [37], which is consistent with the conclusions obtained in Figure 3. The grinding efficiencies of Ca were all higher than 100%, which is opposite to the variation in the grinding efficiency in Figure 3c.

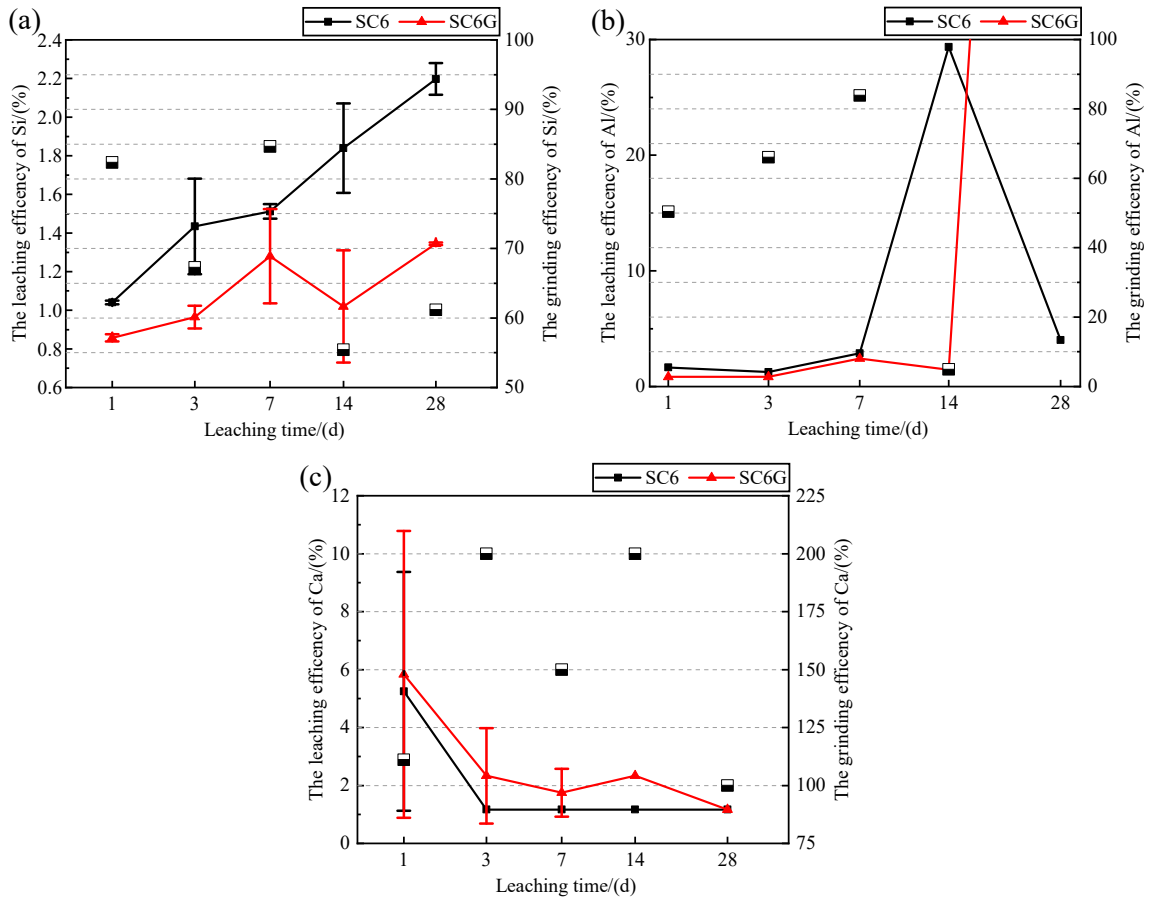

Figure 4. The grinding efficiency between SC6 and SC6G. (**a**) The ion leaching efficiency of Si, (**b**) the ion leaching efficiency of Al, and (**c**) the ion leaching efficiency of Ca. (The plots in the figure correspond to the grinding efficiency on the right axis).

In summary, mechanochemical activation affects the leaching behavior of WPS in alkaline solutions. In terms of the fluctuating variations in ion leaching efficiency, mechanochemical activation accelerates the rate of interaction between the solid surface and the ions in the leachate. In terms of leaching efficiency, mechanochemical activation increases the ion concentration of Si in the leachate after 28 days, and this concentration is affected by the ion concentration of Ca in the leachate, which shows that the ion concentration of Si in the leachate is higher when the ion concentration of Ca is lower. This may be due to the fact that the amount of Ca in the leachate is too insufficient to continue the reaction with the residual Si in the leachate to form gelling-like substances. Therefore, in the modification stage of WPS, the samples subject to mechanochemical activation should be mixed with mineral admixtures that can be calcium sources to make the reaction more adequate.

3.3. Effect of NaOH Concentration on the Dissolution of Si, Al, and Ca

The SG samples were immersed in different concentrations of NaOH solutions curing at 20 °C, and the variation in the leaching efficiencies of Si, Al, and Ca as a function of leaching time was observed, as shown in Figure 5. It can be seen that the leaching efficiency of Si showed an increasing trend with the leaching time but did not increase with the improvement in the concentration of the NaOH solutions. For example, when the leaching time was 28 days, the leaching efficiency of Si corresponding to the 0.5 and 2.0 M NaOH solutions was 1.02% and 0.91%, respectively, and only the leaching efficiency of Si corresponding to 5.0 M NaOH solutions was 4.46%, which was greatly improved.

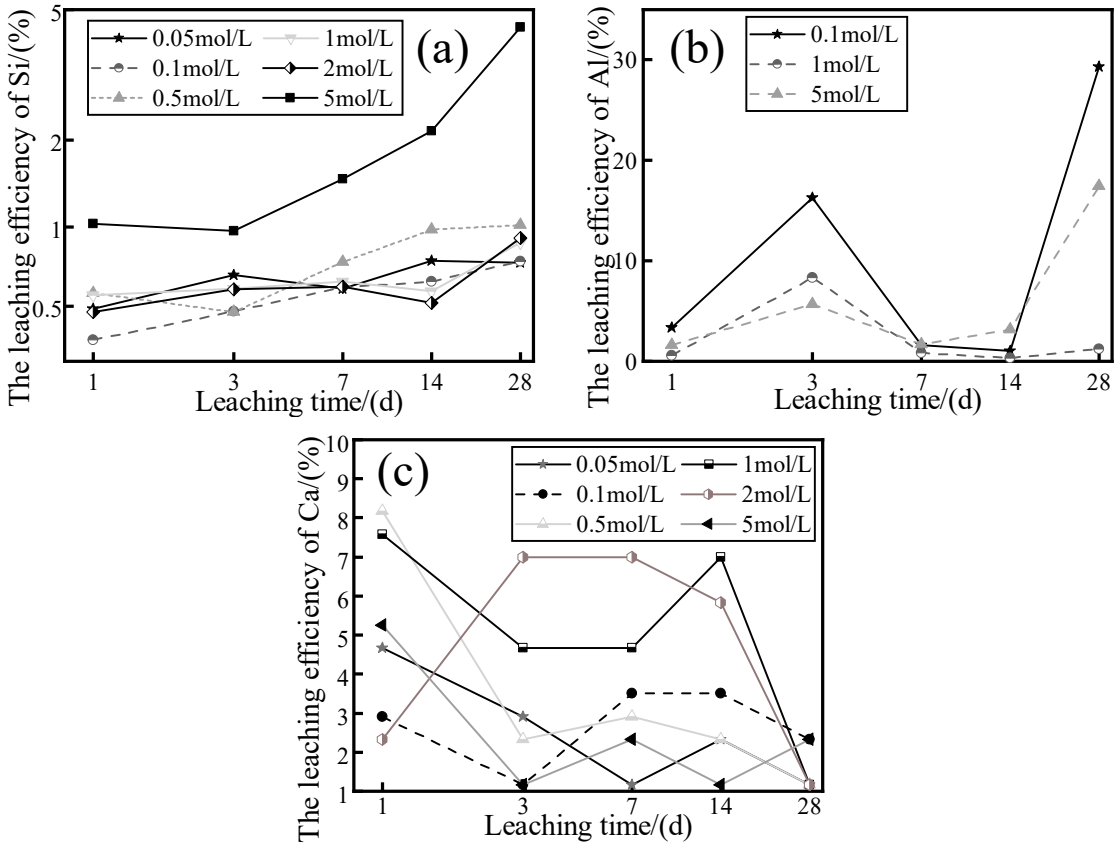

Figure 5. The effect of the concentration of NaOH solutions on the ion leaching efficiency. (**a**) The ion leaching efficiency of Si, (**b**) the ion leaching efficiency of Al, and (**c**) the ion leaching efficiency of Ca.

As shown in Figure 5b, all the curves showed fluctuating variations, exhibiting an increasing trend between 1 and 3 days, a decreasing trend between 3 and 7 days, and an increasing trend between 14 and 28 days. The Al leaching efficiency of 28 days was 27.7, 4.2, and 5.5 of Al leaching efficiency at a leaching time of 14 days, respectively, as the concentration of the leaching agent increased. There was no significant correlation between the concentration of NaOH solutions and the Al leaching efficiency in terms of the difference in the curves. In Figure 5c, it is observed that each curve shows fluctuating variations with different trends from each other.

NaOH solutions of various concentrations represent the concentration of free OH^- ions present in the solution, and this concentration affects the leaching efficiency or dissolution rate and the adsorption and desorption of ions [39]. However, due to the diversity of mineral species in WPS, the interaction between each mineral and the OH^- ion varies, which leads to considerable complexity in the variation in the concentration of each ion in the leachates. Therefore, the variations in ion leaching efficiency are not enough to understand the dissolution characteristics of WPS in alkaline solutions and need to be combined with the mineral composition of the solid residues after leaching.

The XRD of the residues is shown in Figure 6. The montmorillonite peaks of WPS all disappeared after leaching in alkaline solutions with different concentrations, accompanied by an increase in the intensity of diffraction peaks of albite (a feldspar) and muscovite, consistent with the literature [35], which pointed out that albite and muscovite are helpful indicators of montmorillonite decomposition.

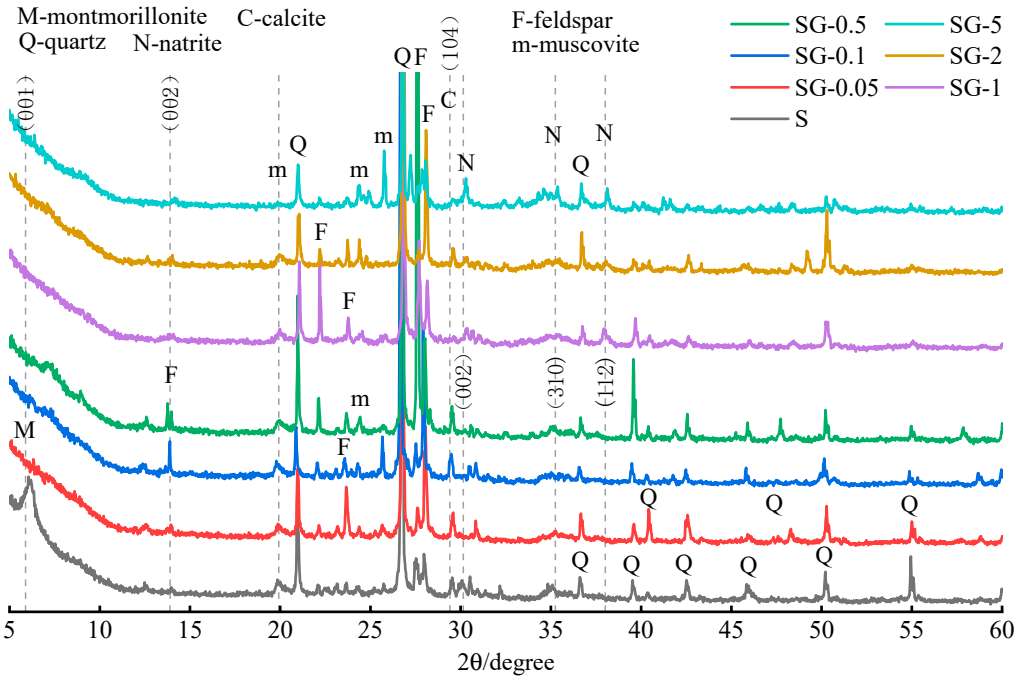

Figure 6. XRD of the residues after leaching. (SG-#: the mechanochemically activated WPS was immersed in a solution of # M NaOH for 28 days, the value of # was 0.05, 0.1, 0.5, 1.0, 2.0, and 5.0, respectively; S: WPS sample immersed in distilled water for 28 days).

A new feldspar peak was observed at 13.9° 2θ when the concentration of the leaching agent was 0.1 and 0.5 M, but this diffraction peak disappeared as the concentration of the leaching agent increased. This may be due to the fact that when the OH^- concentration is higher, it is converted to other substances or exists in an amorphous form. It was observed that the intensity of the diffraction peaks between 27.5° 2θ and 28.5° 2θ tended to increase and then decrease as the concentration of the leaching agent increased. This may be due to the fact that when the concentration of OH^- in the solution is low, the mineral surface is dissolved, and feldspar-like substances are formed. At this time, the concentration of OH^- in the solution is in equilibrium with these substances. However, when the concentration of OH^- in the solution is further increased, these substances react further with OH^-, possibly converting to amorphous substances or disintegrating at higher OH^- [40]. These phenomena seem to explain that, as observed previously, the variation in the leaching efficiency of Si, Al, and Ca does not show a certain regularity with increasing the concentration of the leaching solution.

It can also be observed from Figure 6 that SG-0.5 and SG-1 have excellent material crystallinity, while SG-5 is relatively weak. This phenomenon can explain the considerable increase in the leaching efficiency of Si corresponding to the 5.0 M NaOH solution in Figure 5a. That is, the excessive OH^- ions in the solution interact with the silica–oxygen tetrahedra on the lattice of silicate minerals, Si-O breaks, and Si dissolves into the bulk of the solution in the form of ions or complexes [33]. In addition, three characteristic peaks (30.1° 2θ, 35.3° 2θ, 38.0° 2θ) of natrite (Na_2CO_3) were retrieved at SG-5, which may be the precipitation of excess NaOH during the drying process, which was subsequently carbonated to produce Na_2CO_3 [41]. When the concentration of the leaching agent is low ($\leq$0.5 M), calcite peaks can be observed. However, they disappear at higher concentrations.

In summary, WPS can dissolve more ions in higher concentrations of a NaOH solution. However, when the concentration of the NaOH solution is too high, it will have a negative effect, which will be manifested as a reduction in the crystallinity of the mineral, and more Si/Al/Ca ions will be leached out, while these residual ions are not involved in the generation of new substances and are consumed. In addition, excess alkali will be carbonized after drying to produce sodium carbonate crystals, which can lead to porosity

on the surface of the modified specimens. When the concentration of the NaOH solution is 0.5 and 1 M, the amount of Al and Ca ions leached is well enhanced and can be consumed with sufficient participation in the formation of new substances, as well as having a better mineral crystallinity compared to other concentrations. Therefore, in the modification process of WPS, the concentration of alkaline solution should not be too high, around 1 M is sufficient.

3.4. Effect of Thermal Activation on the Dissolution of Si, Al, and Ca

The calcined WPS samples at different temperatures were immersed in 1.0 M NaOH solutions curing at 20 °C, and the variation in ion leaching efficiency as a function of leaching time was observed, as shown in Figure 7. It can be seen that the leaching efficiency of Si was significantly higher for the thermally activated WPS compared to the SG. The leaching efficiency of Si corresponding to SG, SC6G, SC7G, and SC8G was 0.89%, 1.34%, 2.58%, and 10.32% at 28 days, respectively. It is not difficult to derive from this that the leaching efficiency of Si increased with the increase in calcination temperature. It is worth noting that the variation in the corresponding curve of SG is flatter than the other curves, and the extreme difference in each observation point on the curve is 0.32%. The extreme differences of 0.56%, 1.54%, and 9.56% for each observation point on the corresponding curves of SC6G, SC7G, and SC8G, respectively, indicate that the volatility in the Si leaching efficiency variation becomes more significant with increasing calcination temperature. This may be due to the amorphization of minerals caused by thermal activation [35], which converts minerals to the glassy form and subsequently allows Si to dissolve out of the minerals more easily.

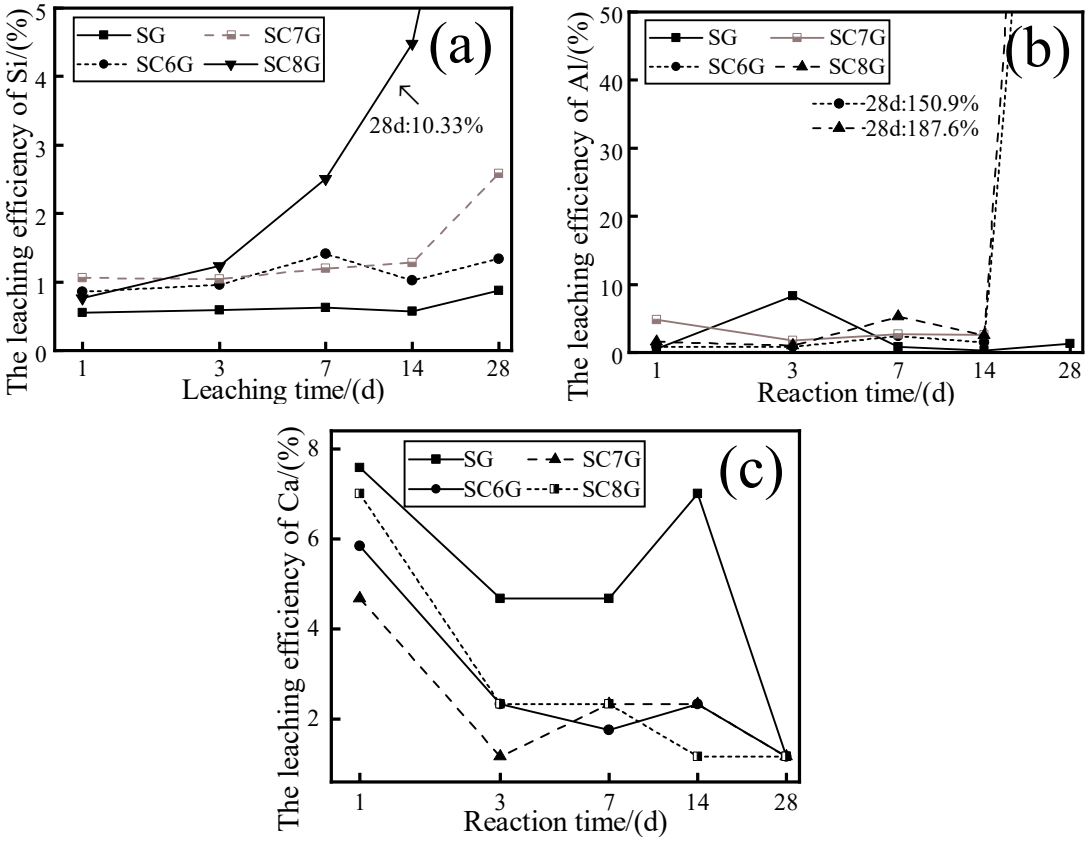

Figure 7. The effect of different temperatures of thermal activation on the leaching efficiency. (**a**) The ion leaching efficiency of Si, (**b**) the ion leaching efficiency of Al, and (**c**) the ion leaching efficiency of Ca.

In Figure 7b, it is observed that each curve shows a fluctuating change before 14 days. At 28 days, the curves corresponding to SC6G and SC8G had a significant increase, and the Al leaching efficiencies of SC6G and SC8G were 150.9% and 187.6%, respectively. SC7G is not plotted due to missing data. It can be seen from Figure 7c that the leaching efficiency of Ca was lower for the thermally activated WPS compared to the SG. In addition, the leaching efficiency of Ca for each curve was 1.67% when the leaching time was 28 days.

The XRD of the residues is shown in Figure 8. It can be seen that the intensity of the diffraction peaks of the feldspar and muscovite species between 22.0° 2θ and 26.4° 2θ is affected by the calcination temperature. The intensity of the partial diffraction peaks (22.0° 2θ) gradually decreased with increasing calcination temperature, and the intensity of the partial diffraction peaks (23.7° 2θ) gradually increased with increasing calcination temperature. The intensity of the diffraction peaks for feldspar species between 27.5° 2θ and 28.5° 2θ is also affected by the calcination temperature. These phenomena can be explained as follows.

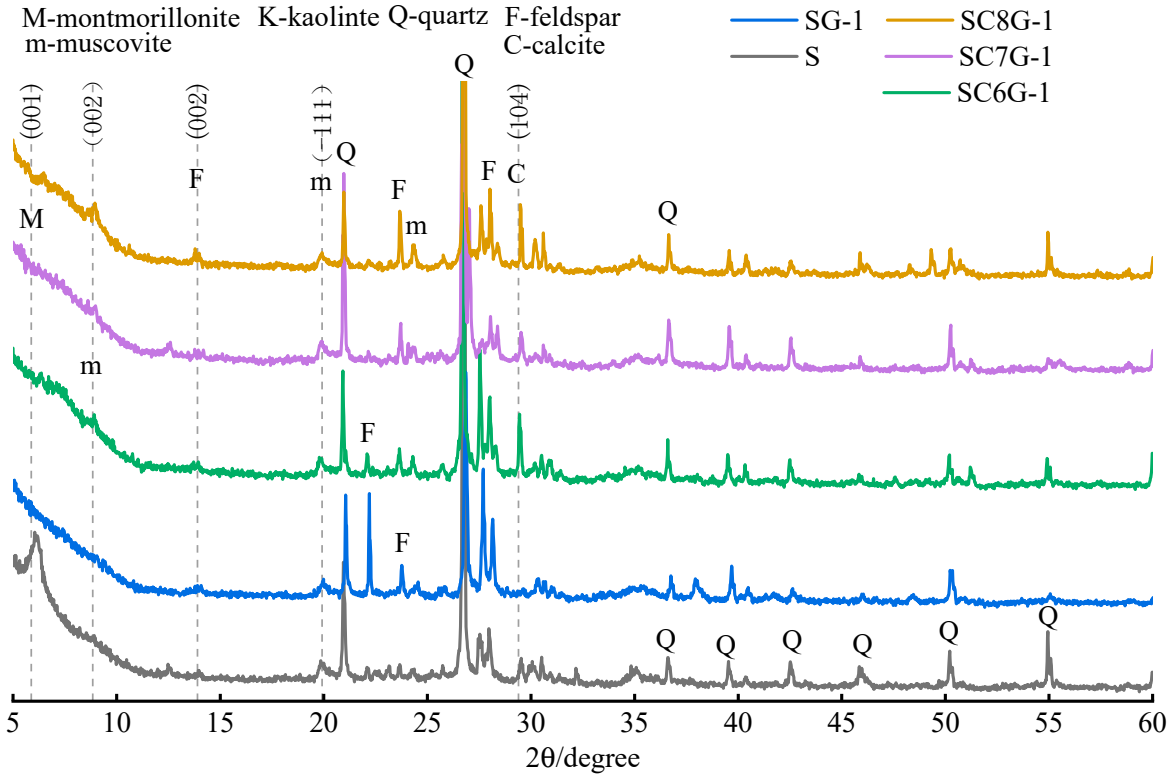

Figure 8. XRD of the residues after leaching. (SC*G: the thermally and mechanochemically activated WPS was immersed in a solution of 1.0 M NaOH for 28 days, and the value of * was the temperature of thermal activation; S: WPS sample immersed in distilled water for 28 days).

It has been concluded from Figure 2 that thermal and mechanochemical activation caused the amorphization of the minerals in WPS into the glassy state, while increasing the surface chemical energy and improving the chemical reactivity [34]. Subsequently, the glassy material can develop and reorganize well in alkaline solutions. Therefore, the difference between the spectral lines in Figure 8 is mainly caused by the calcination temperature. In addition, the intensity of the diffraction peak of anorthite sodian (a feldspar) at 13.9° 2θ varies with the change in calcination temperature, but there is no certain rule. It has been observed from Figure 2 that the diffraction peak of calcite at 29.4° 2θ almost disappears at high temperatures; however, it is detected in Figure 8. This seems to explain that the leaching efficiency of Ca for 28 days corresponding to each curve in Figure 7c was maintained at 1.67%.

The crystallinity of feldspar-like minerals and mica-like minerals in the thermally activated WPS was significantly increased after leaching. Before leaching, the crystallinity of the minerals gradually decreased with the increase in the temperature of thermal activation. However, after leaching, the difference in the crystallinity of the minerals of the samples subjected to different thermal activation temperatures was not significant. This may be due to the fact that the increase in the thermal activation temperature can convert more minerals in WPS to glassy or amorphous forms, which makes Si easier to leach in the alkaline solution and increases the ion concentration of Si in the leachate. However, the Si in the leachate is limited by the amount of Ca or other substances, resulting in a portion of Si not being able to further develop and reorganize to generate new substances. Therefore, the higher the thermally activated temperature of the WPS, the more mineral admixtures with available Ca should be added in the modification stage.

3.5. Effect of Curing Temperature on the Dissolution of Si, Al, and Ca

S and SC6G were immersed in 5.0 M NaOH solutions, and their leaching times were 28 days and 3 days at 20 °C and 80 °C, respectively. It is well known that when the temperature increases, the rate of the reaction between the solutes and the solution also increases [37]. To better compare the leaching behavior of the samples at different curing temperatures, the temperature influence rate (*TIR*) was used to characterize the effect of curing temperature on the leaching of each ion, which was calculated as follows:

$$TIR = \frac{H_n - N_B}{N_T - N_B} \times 100\%, n = 0.5, 1, 3d \quad (2)$$

where H_n is the concentration of each ion in the leachate at 80 °C when the leaching time is n, N_T is the maximum value of the concentration of each ion in the leachate when the leaching time is 1, 3, 7, 14, and 28 days at 20 °C, and N_B is the minimum value of the concentration of each ion in the leachate when the leaching time is 1, 3, 7, 14, and 28 days at 20 °C.

As shown in Figure 9a, the *TIR* of Si reaches 87% and 286% at leaching times of 0.5 and 1 day, respectively. The *TIR* of Si corresponding to S-5 was almost twice as high as that of SC6G-5 at a leaching time of 3 days, which is consistent with the conclusion obtained from Figure 7 showing that relative to the untreated WPS, the Si leaching efficiency of the thermally activated WPS has been improved, which makes the increase in TIR of SC6G-5 less than that of S-5. It can also be deduced that the effect of curing temperature on the Si leaching efficiency is greater than that of thermal activation on the Si leaching efficiency. This may be due to the fact that thermal activation favors the activation of raw materials [35]. At the same time, the increase in curing temperature not only accelerates the rate of mineral dissolution [39] but also raises the threshold of ion leaching efficiency.

The TIR of Al is less than 100%, which indicates that the Al leaching efficiency within 3 days of leaching at 80 °C does not exceed the Al leaching efficiency within 28 days of leaching at 20 °C. This may be caused by insufficient leaching time. Figure 5b shows that the Al leaching efficiency increased significantly between 14 and 28 days for each leaching agent concentration, whereas the leaching time at 80 °C was only 3 days, resulting in a lower amount of Al being leached into the leachate. In addition, the TIR of Al in Figure 9a for 3 days is 61%, and that in Figure 9b for 3 days is 34%, indicating that the elevated curing temperature would hasten the rate of Al leaching from the WPS.

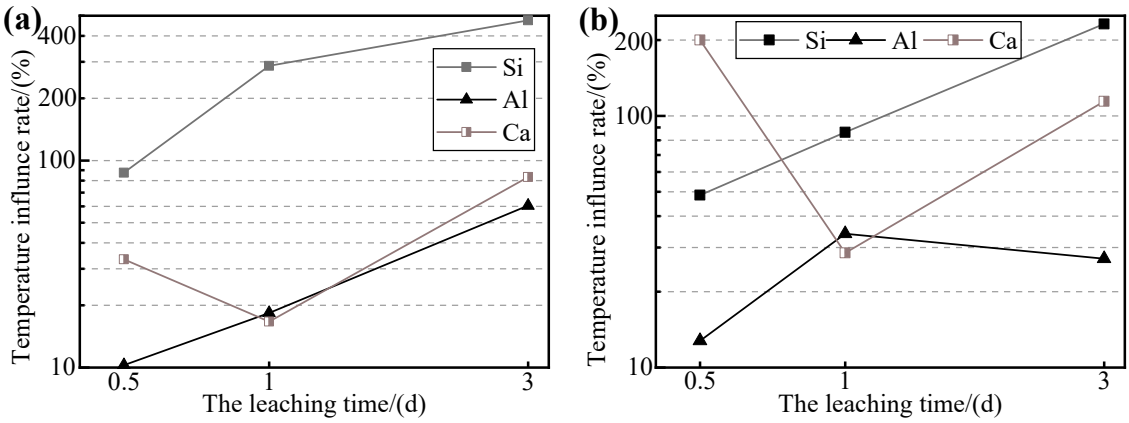

Figure 9. The influence of curing temperature on the ion leaching efficiency. (**a**) WPS was immersed in a solution of 5.0 M NaOH (S-5). (**b**) The mechanochemically and thermally activated WPS was immersed in a solution of 5.0 M NaOH (SC6G-5).

The XRD of the residues after leaching for 28 days at 20 °C and after leaching for 3 days at 80 °C are shown in Figure 10. It was observed that muscovite peaks almost disappeared. This result was compared with muscovite peaks at a relatively low leaching agent concentration (0.5 M) in Figure 8, from which it can be inferred that muscovite will be destroyed in a higher concentration of NaOH solutions. It can be seen from a comparison of S-5 and S-5 (80 °C) that the latter has a higher mineral crystallinity than the former, indicating that the increase in curing temperature may lead to a tendency for the products of the dissolution of minerals to crystallize.

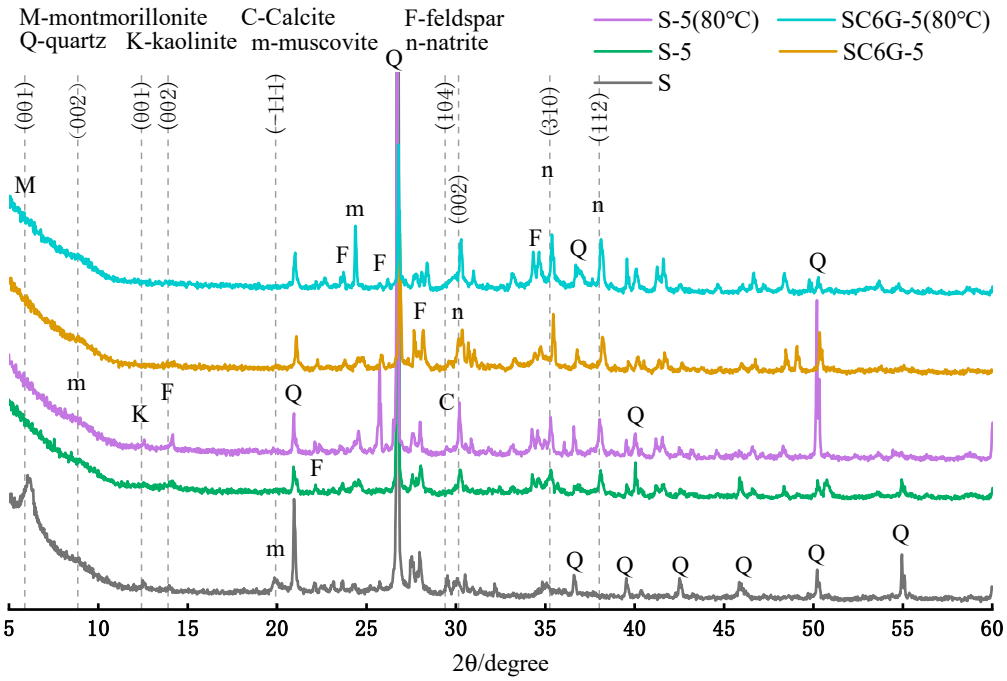

Figure 10. XRD of the residues after leaching. (S: WPS sample immersed in distilled water for 28 days curing at 20 °C; S-5: WPS was immersed in a solution of 5.0 M NaOH for 28 days curing at 20 °C; and S-5 (80 °C): WPS was immersed in a solution of 5.0 M NaOH for 3 days curing at 80 °C).

In addition, the presence of obvious diffraction natrite peaks is observed, which confirms the conclusion obtained in Figure 6. The calcite peaks disappeared when the concentration of the leaching agent was 5.0 M, which is also consistent with the conclusion obtained in Figure 6.

3.6. Microstructure of Residue after Leaching

The SEM image of the partial residues is shown in Figure 11. Their elemental composition was analyzed with EDS, and the relevant data are shown in Table 6. It can be seen from Figure 11a that the surface of WPS is mainly distributed with layered and flaky material, and the particle size is large. The presence of montmorillonite can be observed in Figure 11b, while the data on the atomic percentages are in close agreement with the molecular formula of montmorillonite. It can be observed from the figure corresponding to SG-1 that the surface of the particles seems to be enveloped by dense spherical material, along with a larger number of pores and holes. However, when the concentration of the NaOH solution was 5.0 M, a large number of slender needle-like substances were distributed on the surface of the residues. Combined with the results of the EDS analysis, that is inferred to be natrite, which is consistent with the conclusion obtained from Figure 10. This result was also observed by Bucullo et al. [41]. In addition, it is also observed in Figure 11f that there is a thin layer of material on the surface of the particles, and many holes are distributed on it.

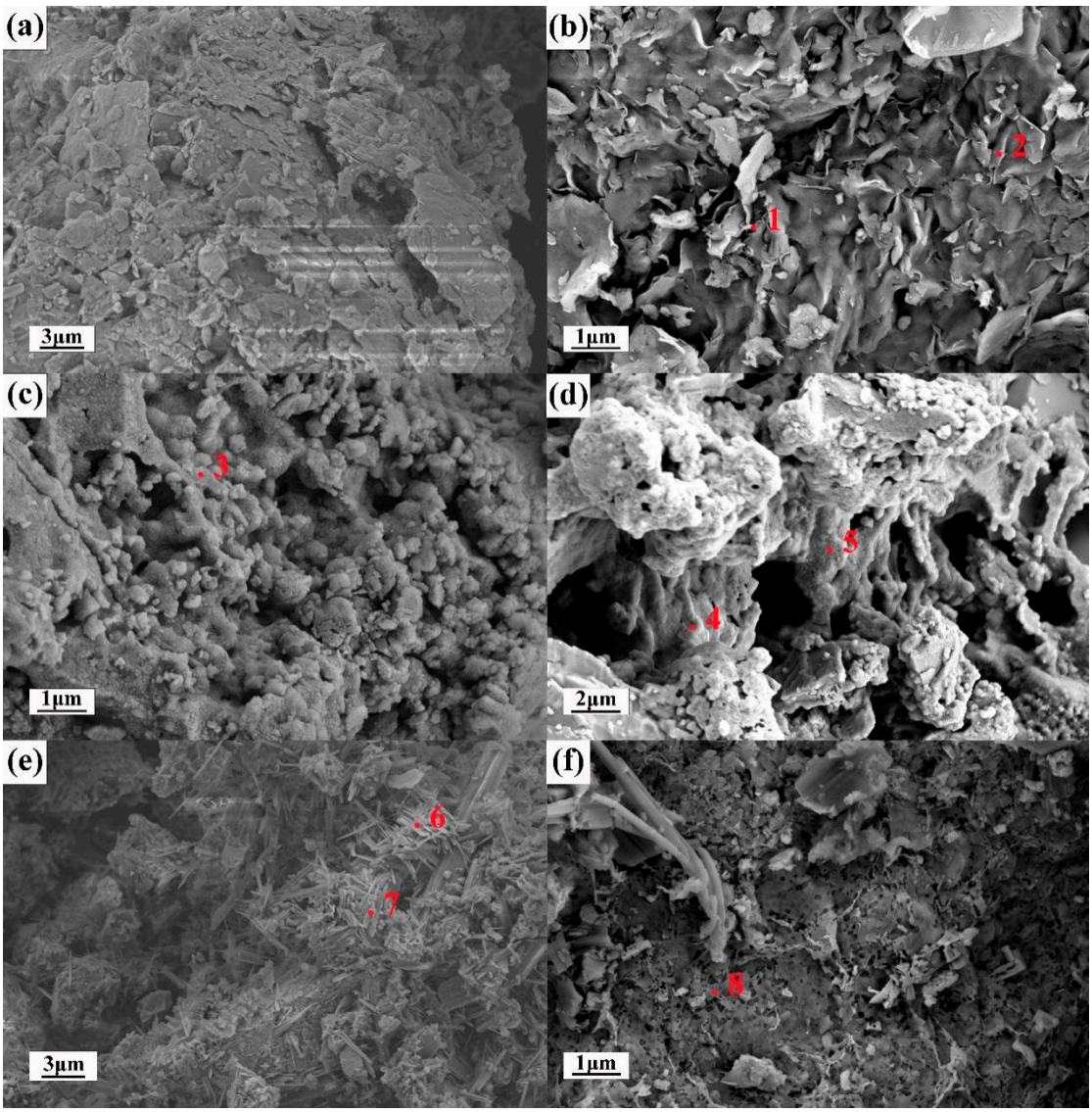

Figure 11. SEM images of samples. (**a**) Mag = 5.0 K X and (**b**) Mag = 5.0 K X samples of S, (**c**) Mag = 20.0 K X and (**d**) Mag = 5.0 K X samples of SG-1, and (**e**) Mag = 5.0 K X and (**f**) Mag = 10.0 K X samples of SC6G-5. (The red plot in figure is used for the SEM-EDS based on point scanning).

Table 6. SEM-EDS of residue after leaching. (Atomic percent %).

Plot	Element						
	C	**O**	**Na**	**Mg**	**Al**	**Si**	**Ca**
1	3.85	60.55	0.08	2.63	8.92	22.87	1.11
2	6.26	59.8	0.04	2.53	8.56	21.39	1.42
3	8.4	51.43	22.61	2.57	2.18	11.78	1.04
4	5.96	37.13	15.78	2.5	3.42	33.42	1.79
5	4.93	41.14	23.45	1.77	7.11	20.2	1.39
6	18.28	45.76	32.29	0.67	0.52	0.97	1.51
7	10.97	41.87	29.89	0.75	3.53	11.89	1.1
8	3.43	56.83	2.05	6.92	7.28	21.36	2.13

4. Conclusions

This work investigated the properties of WPS after leaching in alkaline solutions. The effects of thermal activation, mechanochemical activation, the concentration of NaOH solution, and curing temperature on the leaching efficiency of Si, Al, and Ca were investigated. The composition and microstructure of the residues after leaching were analyzed. The following conclusions can be drawn:

(1) Mechanochemical activation reduced the particle size of the WPS. Mechanochemical activation increases the ion concentration of Si in the leachate after 28 days, and this concentration is affected by the ion concentration of Ca in the leachate. The residual Si in the leachate is limited by the insufficient amount of Ca in the leachate to participate in the precipitation of the newborn minerals and is consumed. In the modification stage of WPS, the mechanochemically activated sample should be mixed with mineral admixtures available as a calcium source to make the interaction more adequate.

(2) WPS can dissolve more ions in higher concentrations of a NaOH solution. When the concentration of the NaOH solution is 5 M, there is a negative effect that the crystallinity of the mineral will be reduced and more ions will be leached out, while these residual ions in the leachate are not consumed to participate generation of new substances. In addition, excess alkali will be carbonized after drying to produce sodium carbonate crystals, which can lead to porosity on the surface of the modified specimens. When the concentration of NaOH solution is 0.5 and 1 M, the amount of Al and Ca ions leached is well enhanced and can be consumed with sufficient participation in the generation of new substances as well as having a better mineral crystallinity compared to other concentrations. Therefore, in the modification stage of WPS, the concentration of alkaline solution should not be too high, around 1 M is sufficient.

(3) The crystallinity of feldspar-like minerals and mica-like minerals in the thermally activated WPS was significantly increased after leaching. Before leaching, the crystallinity of the minerals gradually decreased with the increase in the temperature of thermal activation. However, after leaching, the difference in the crystallinity of the minerals of the samples subjected to different thermal activation temperatures was not significant. This may be due to the fact that the increase in the thermal activation temperature can convert more minerals in WPS to glassy or amorphous forms, which makes ions easier to leach in the alkaline solution. However, the Si in the leachate is limited by the amount of Ca or other substances, resulting in a portion of Si not being able to further develop and reorganize to generate new substances. Therefore, the higher the thermally activated temperature of the WPS the more mineral admixtures with available Ca should be added in the modification stage.

(4) The increase in the curing temperature will promote the interaction between WPS and the alkaline solution. Higher curing temperatures can greatly increase the ion leaching efficiency of Si in a short period of time, and its effect is better than thermal activation. At the same time, it also promotes the generation of newborn minerals

and increases the crystallinity of minerals in WPS after leaching. Therefore, higher curing temperatures of modified WPS specimens will facilitate the development of specimens.

Author Contributions: Writing—original draft preparation, C.L.; data curation, H.C. and Y.C.; writing—review and editing, S.Z. and C.Y.; investigation, C.D. and D.J. All authors have read and agreed to the published version of the manuscript.

Funding: The authors would like to express gratitude for the financial support from the National Natural Science Foundation of China (51708216), Key Projects of Science and Technology of Henan Province (192102310223), Open project of Henan Key Laboratory of Ecological Environment, Protection and Restoration of Yellow River Basin (LYBEPR202104), the Technology development project of Power Construction Corporation of China, Henan Wanshan Green Building Materials Co. LTD (ZDJWS-2022-004), and the Fund of Innovative Education Program for Graduate Students at North China University of Water Resources and Electric Power (YK-2021-04).

Data Availability Statement: Data obtained as described.

Conflicts of Interest: The authors declare no conflict of interest.

References

1. Song, T.; Liu, L.; Wang, Y.; Liu, N.; Yu, M. Characteristics and genesis of the bleached Pisha sandstone in Ordos Basin. *Oil Gas Geol.* **2014**, *35*, 679–684. (In Chinese)
2. Li, C.; Song, L.; Cao, Y.; Zhao, S.; Liu, H.; Yang, C.; Cheng, H.; Jia, D. Investigating the Mechanical Property and Enhanced Mechanism of Modified Pisha Sandstone Geopolymer via Ion Exchange Solidification. *Gels* **2022**, *8*, 300. [CrossRef]
3. Li, C.; Dong, J.; Zhao, S.; Liu, H.; Yao, W.; Wang, L. Development of low cost supplementary cementitious materials utilizing thermally activated Pisha sandstone. *Constr. Build. Mater.* **2018**, *174*, 484–495. [CrossRef]
4. Li, C.; Zhang, T.; Wang, L. Mechanical properties and microstructure of alkali activated Pisha sandstone geopolymer composites. *Constr. Build. Mater.* **2014**, *68*, 233–239. [CrossRef]
5. Ye, H.; Shi, J.; Li, X.; Hou, H.; Shi, Y.; Cheng, Y. The Effect of Soft Rock Lithology upon Its Anti-erodibility. *Acta Geosci. Sin.* **2006**, *27*, 145–150. (In Chinese)
6. Wang, L.; Li, C.; Dong, J. Study on Distribution and Lithologic Characters of Feldspathic Sandstone. *Yellow River* **2013**, *35*, 91–93. (In Chinese)
7. Li, C.; Song, L.; Wang, L. Mineral composition and anti-erodibility of Pisha sandstone. *Sci. Soil Water Conserv.* **2015**, *13*, 11–16. (In Chinese)
8. Shi, Y.; Ye, H.; Hou, H.; Bi, Z. The internal cause of the erosion in Pisha sandstone area in Southern inner Mongolia. *Acta Geosci. Sin.* **2004**, *25*, 659–664. (In Chinese)
9. Yang, J.; Fang, D.; Bi, C.; Qiao, W.; Li, G.; Li, W. Action of Seabuckthorn in Freeze-thaw and Weathering Erosion of Small Watershed in Soft Rock Area. *J. Soil Water Conserv.* **2002**, *4*, 41–44. (In Chinese)
10. Wang, Y.; Wu, Y.; Kou, Q.; Min, D.; Chang, Y.; Zhang, R. Definition of arsenic rock zone borderline and its classification. *Sci. Soil Water Conserv.* **2007**, *5*, 14–18. (In Chinese)
11. Bi, C.; Wang, F.; Li, X. Field Test of Seabuckthorn Plant Flexible Dam in Arsenic Sandstone Area. *Soil Water Conserv. China* **2022**, *4*, 46–52. (In Chinese)
12. Xiao, P.; Yao, W.; Liu, H. Research Progress and Harnessing Method of Soil and Water Loss in Pisha sandstone Region. *Yellow River* **2014**, *36*, 92–94. (In Chinese) [CrossRef]
13. Gao, Z.; Yang, S. Existing Problems of Silt Arresters on the Loess Plateau. *Bull. Soil Water Conserv.* **1999**, *6*, 16–19. (In Chinese)
14. Li, C.; Wang, L.; Yang, D.; Zhang, T.; Han, J.; Dong, J. Characters of Montmorillonite of Pisha sandstone. *Yellow River* **2016**, *38*, 11–14. (In Chinese)
15. Li, C.; Wang, L.; Zhang, T.; Dong, J. Development of building material utilizing a low pozzolanic activity mineral. *Constr. Build. Mater.* **2016**, *121*, 300–309. [CrossRef]
16. Li, C.; Zhang, T.; Wang, L. Effect of dosage of fly ash and NaOH on the properties of alkali activated Pisha sandstone-based mortar. *ACI Mater. J.* **2016**, *113*, 173–183.
17. Li, C.; Zhang, T.; Wang, L. Pozzolanic activity of Pisha sandstone and mechanical properties of alkali-activated Pisha sandstone materials. *J. Chin. Ceram. Soc.* **2015**, *43*, 1090–1098. (In Chinese)
18. Yang, D.; Zhang, T.; Han, J.; Dong, J.; Li, C.; Wang, L. Study of Building Check Dam by Using Modified Pisha sandstone. *Yellow River* **2016**, *38*, 42–45. (In Chinese)
19. Petrus, H.T.B.M.; Olvianas, M.; Shafiyurrahman, M.F.; Pratama, I.G.A.A.N.; Jenie, S.N.A.; Astuti, W.; Nurpratama, M.I.; Ekaputri, J.J.; Anggara, F. Circular Economy of Coal Fly Ash and Silica Geothermal for Green Geopolymer: Characteristic and Kinetic Study. *Gels* **2022**, *8*, 233. [CrossRef]

20. Sofi, M.; van Deventer, J.; Mendis, P.; Lukey, G. Engineering properties of inorganic polymer concretes (IPCs). *Cem. Concr. Res.* **2007**, *37*, 251–257. [CrossRef]
21. Kljajević, L.; Nenadović, M.; Ivanović, M.; Bučevac, D.; Mirković, M.; Nikolić, N.M.; Nenadović, S. Heat Treatment of Geopolymer Samples Obtained by Varying Concentration of Sodium Hydroxide as Constituent of Alkali Activator. *Gels* **2022**, *8*, 333. [CrossRef] [PubMed]
22. Yao, G.; Cui, T.; Zhang, J.; Wang, J.; Lyu, X. Effects of mechanical grinding on pozzolanic activity and hydration properties of quartz. *Adv. Powder Technol.* **2020**, *31*, 4500–4509. [CrossRef]
23. Yao, G.; Wang, Z.; Yao, J.; Cong, X.; Anning, C.; Lyu, X. Pozzolanic activity and hydration properties of feldspar after mechanical activation. *Powder Technol.* **2021**, *383*, 167–174. [CrossRef]
24. Vizcayno, C.; de Gutiérrez, R.M.; Castello, R.; Rodriguez, E.; Guerrero, C. Pozzolan obtained by mechanochemical and thermal treatments of kaolin. *Appl. Clay Sci.* **2010**, *49*, 405–413. [CrossRef]
25. Luukkonen, T.; Abdollahnejad, Z.; Yliniemi, J.; Kinnunen, P.; Illikainen, M. One-part alkali-activated materials: A review. *Cem. Concr. Res.* **2018**, *103*, 21–34. [CrossRef]
26. Topolska, J.; Puzio, B.; Borkiewicz, O.; Sordy, J.; Manecki, M. Solubility Product of Vanadinite Pb5(VO4)3Cl at 25 °C—A Comprehensive Approach to Incongruent Dissolution Modeling. *Minerals* **2021**, *11*, 135. [CrossRef]
27. Yang, F.; Li, Q.; Wang, D.; Zhou, C.; Zheng, S. Interfacial Structure Change and Selective Dissolution of Columbite–(Fe) Mineral during HF Acid Leaching. *Minerals* **2021**, *11*, 146. [CrossRef]
28. Yuan, J.; Ma, H.; Luo, Z.; Ma, X.; Guo, Q. Synthesis of $KAlSiO_4$ by Hydrothermal Processing on Biotite Syenite and Dissolution Reaction Kinetics. *Minerals* **2020**, *11*, 36. [CrossRef]
29. House, W.A.; Orr, D.R. Investigation of the pH dependence of the kinetics of quartz dissolution at 25 °C. *J. Chem. Soc. Faraday Trans.* **1992**, *88*, 233–241. [CrossRef]
30. Gitari, W.M.; Fatoba, O.O.; Petrik, L.F.; Vadapalli, V.R. Leaching characteristics of selected South African fly ashes: Effect of pH on the release of major and trace species. *J. Environ. Sci. Heal. Part A* **2009**, *44*, 206–220. [CrossRef] [PubMed]
31. Terry, B. The acid decomposition of silicate minerals part II. Hydrometallurgical applications. *Hydrometallurgy* **1983**, *10*, 151–171. [CrossRef]
32. Terry, B. Specific chemical rate constants for the acid dissolution of oxides and silicates. *Hydrometallurgy* **1983**, *11*, 315–344. [CrossRef]
33. Crundwell, F.K. The mechanism of dissolution of minerals in acidic and alkaline solutions: Part II Application of a new theory to silicates, aluminosilicates and quartz. *Hydrometallurgy* **2014**, *149*, 265–275. [CrossRef]
34. Souri, A.; Kazemi-Kamyab, H.; Snellings, R.; Naghizadeh, R.; Golestani-Fard, F.; Scrivener, K. Pozzolanic activity of mechanochemically and thermally activated kaolins in cement. *Cem. Concr. Res.* **2015**, *77*, 47–59. [CrossRef]
35. Fernandez, R.; Martirena, F.; Scrivener, K.L. The origin of the pozzolanic activity of calcined clay minerals: A comparison between kaolinite, illite and montmorillonite. *Cem. Concr. Res.* **2011**, *41*, 113–122. [CrossRef]
36. Song, T.; Tian, Z.; Liu, L.; Wang, S.; Wang, J. Dissolution of Acetic Acid Solution of Alkali Feldspar and Study on Its Numerical Simulation. *Mineral Petrol.* **2017**, *37*, 1–5. (In Chinese)
37. Crundwell, F.K. The mechanism of dissolution of minerals in acidic and alkaline solutions: Part I—A new theory of non-oxidation dissolution. *Hydrometallurgy* **2014**, *149*, 252–264. [CrossRef]
38. Skrobian, M.; Havlik, T.; Ukasik, M. Effect of NaCl concentration and particle size on chalcopyrite leaching in cupric chloride solution. *Hydrometallurgy* **2005**, *77*, 109–114. [CrossRef]
39. Faraji, F.; Alizadeh, A.; Rashchi, F.; Mostoufi, N. Kinetics of leaching: A review. *Rev. Chem. Eng.* **2020**, *38*, 113–148. [CrossRef]
40. Lin, P.; Zeng, L.; He, D.; Ding, Y. Reaction and Its Kinetics of Montmorillonite, Quartz with Alkaline Solution. *Chem. Eng. Oil Gas* **2002**, *31*, 144–149. (In Chinese)
41. Bocullo, V.; Vitola, L.; Vaiciukyniene, D.; Kantautas, A.; Bajare, D. The influence of the SiO2/Na2O ratio on the low calcium alkali activated binder based on fly ash. *Mater. Chem. Phys.* **2021**, *258*, 123846. [CrossRef]